Rotational Motion of Alkanes on Zeolite ZK-5 Studied from $^1H-^{13}C$ NMR Cross-Relaxation

Vadim E. Zorine, Pieter C. M. M. Magusin,* and Rutger A. van Santen

Schuit Institute of Catalysis, Laboratory of Inorganic Chemistry and Catalysis, Eindhoven University of Technology, P.O. Box 513, Eindhoven, The Netherlands

Received: May 24, 2003; In Final Form: December 24, 2003

We have studied the rotational mobility of a mixture of butane and pentane on zeolite ZK-5 as a function of temperature from $^1H-^{13}C$ cross-relaxation at 4.7 and 11.7 T. In the studied temperature range (130−320 K), the sorbed alkanes are practically confined inside the α and γ cages of ZK-5. This is confirmed by well-resolved peaks in magic-angle-spinning (MAS) ^{13}C NMR spectra for each alkane in each cage. Despite the translational confinement, the observed NMR relaxation for the methylene groups of butane and pentane reflects extensive rotational motion inside cages. The maximum cross-relaxation rates indicate a combination of ultrafast rotation about the alkane axis (including internal bond rotations) and a slower tumbling of the molecular axis itself. Two temperature regimes can be distinguished. Above 200 K, the effective tumbling times derived from the initial cross-relaxation show Arrhenius behavior with activation energies between 5 and 15 kJ/mol. Below 200 K, the motion becomes less activated. We consider various possible explanations and discuss three models: (A) a combination of activated and nonactivated motion, (B) a Gaussian distribution of activation energies, (C) concerted sorbate−zeolite motions. Model C involves a flexible zeolite lattice, which accommodates the binding of molecules by small dynamic deformations.

Introduction

The dynamics of molecules adsorbed in the pore network of zeolites and other molecular sieves is an important topic in catalysis. Molecular motions directly control the transport of reactants and products in zeolite-catalyzed reactions and may even be rate-determining for the overall reaction. Indirectly, the partial immobilization of adsorbed molecules yields insight into the sorbate−zeolite binding interactions, which underlie the chemical activation of molecules inside zeolites. We here report an $^1H-^{13}C$ NMR cross-relaxation study of the rotational mobility of butane and pentane adsorbed on zeolite ZK-5. This zeolite has two types of cages, α and γ,[1] accessible to pentane and butane (Figure 1).[2,3] The observed cross-relaxation as a function of temperature reveals detailed information about the time scale and activation energy of the underlying molecular motion.

Among a few other experimental techniques, like inelastic neutron scattering[4] and dielectric spectroscopy,[5] NMR spectroscopy is a powerful tool to study sorbate motion on zeolites over a broad range of time scales, $10^{-12}-10^{1}$ s. By use of externally applied magnetic-field gradients, self-diffusion can be studied down to 10^{-11} m^2/s at a micrometer scale in zeolites.[6] Intracage and intercage hopping of deuterated benzene in Na−Y on a time scale between 10^{-4} and 10^{-3} s has been investigated with ^2H NMR.[7] Using the chemical-shift differences between various cage environments, hopping of pentane in zeolite ZK-5 as the elementary step of even slower self-diffusion ($10^{-18}-10^{-15}$ m^2/s) can be observed.[3] Longitudinal NMR (cross-)-relaxation yields information about sorbate rotation in the range $10^{-12}-10^{-8}$ s. The work presented in this article is related to that by Michel and co-workers.[8,9] They have studied ^1H spin−lattice relaxation, as well as $^1H-^1H$ and (steady-state) $^1H-^{13}C$ cross-relaxation for small olefins on zeolite NaX at a single temperature (300 K) and field (11.7 T). For our system, a butane/pentane mixture on ZK-5, ^1H NMR spectroscopy does not yield sufficient resolution, and ^1H NMR relaxation is strongly affected by spin diffusion. We have therefore focused on the transient $^1H-^{13}C$ cross-relaxation observed in the magic-angle-spinning ^{13}C NMR spectrum immediately after inversion of the proton spins. In this way we obtain separate mobility information for butane and pentane in each of the two cage types under exactly the same experimental conditions. As a consistency check, the measurements were carried out in two different magnetic fields. The temperature was varied to obtain insight into rotational activation barriers and possible deviations from Arrhenius behavior. Detailed information on the microscopic mobility of adsorbed molecules in zeolites can help to understand the sorbate−zeolite interactions inside the cavities.

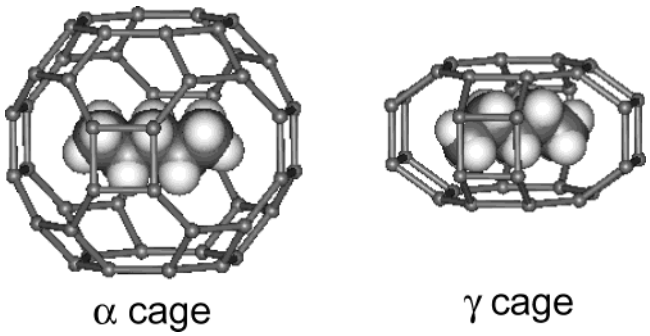

Figure 1. α and γ cage of zeolite ZK-5 with a single pentane molecule to illustrate the relative dimensions. For the cages, the silicon positions are indicated only. These are bridged by oxygen atoms, which dominate the van der Waals interaction with the adsorbed alkane. The α cage has cubic symmetry, and the γ cage, C_4 symmetry (major axis vertically in the plane of the paper).

General NMR relaxation theory relates relaxation rates to the rotational spectral density of the molecules in the Larmor frequency range (10^8-10^9 Hz) and is valid for molecules tumbling fast on the dipolar time scale (10^{-4} s).[10] This condition is readily fulfilled for small molecules in solution, and in liquids, NMR (cross-)relaxation is often measured to obtain information

10.1021/jp0354447 CCC: $27.50 © 2004 American Chemical Society
Published on Web 04/14/2004

about the hydrodynamic size of molecules in viscous media[10] or sidegroup mobility at the surface of a protein.[11,12] For solid or semisolid systems, NMR relaxation is less routinely used to study motion for a number of reasons. First, motions with correlation times at the Larmor time scale tend to be absent or have small amplitudes in solids. The resulting intrinsic relaxation is generally slow and then readily contaminated by other mechanisms not related to molecular motion. For example, proton spin−lattice relaxation in polymers is strongly affected by spin diffusion and reflects spatially averaged rather than local chain mobility. Second, a more fundamental problem is the incomplete rotational motion of molecules in a solid, as a result of which residual-order effects may arise. For instance, chemically identical spin systems with different residual orientations relative to the magnetic field may relax with different rates, a phenomenon called relaxation anisotropy.[13] Third, due to the lack of translational and conformational averaging in solids heterogeneity effects often show up for amorphous systems, which may complicate the interpretation of NMR relaxation.

In our present NMR study of butane and pentane on zeolite ZK-5, we have tried to avoid the above complications as much as possible. The alkane molecules undergo large-amplitude rotations inside the zeolite cavities, resulting in relatively fast relaxation in the temperature range studied. Moreover, we focus on ^{1}H−^{13}C cross-relaxation, on which spin diffusion has no direct influence, because the difference between the ^{1}H and ^{13}C NMR frequency exceeds the dipolar coupling by at least 4 orders of magnitude. Relaxation anisotropy is suppressed by applying magic-angle spinning (MAS), a common line-narrowing technique in solid-state NMR involving mechanical rotation of the sample about a specific angle (54.7°) with respect to the magnetic field. Using MAS we are also able to discriminate between the signals of butane and pentane in each of the two cage types, α and γ, in ZK-5. Since zeolites are well-defined crystallites with highly regular cavities, heterogeneity effects should be minimal, especially for the γ cage, which can contain no more than a single butane or pentane molecule.

Theory

Stochastic reorientation of the internuclear ^{13}CH vectors in a hydrocarbon molecule causes random fluctuations of the dipolar ^{13}CH interaction, which, in turn, lead to NMR relaxation. Detailed relaxation theory for $^{13}CH_n$ spin systems ($n = 1, 2, 3$) has been developed by Grant and others.[14] After a perturbation of the proton polarization, the ^{13}C polarization $I(\tau)$ is transiently enhanced in a biexponential way, $I^{eq} + (S(0) - S^{eq})\,\sigma_{CH}\{\exp(-\lambda_1\tau) - \exp(-\lambda_2\tau)\}/(\lambda_2 - \lambda_1)$ with I^{eq} as the ^{13}C equilibrium polarization, $S(0) - S^{eq}$ as the initial proton perturbation, and λ_1 and λ_2 as two eigenvalues of the so-called Redfield matrix for a $^{13}CH_n$ spin system.[14] Here we focus on the initial rates σ_{CH} of transient ^{1}H−^{13}C cross-relaxation after an ^{1}H perturbation in a $^{13}CH_2$ system originally in thermal equilibrium. ^{1}H and ^{13}C spin−lattice relaxation, which are more frequently measured to determine rotational motion, tend to be contaminated by other relaxation mechanisms, such as induced by spin diffusion and chemical shift anisotropy. In contrast, the initial cross-relaxation rate purely arises from the well-defined dipolar ^{1}H−^{13}C interactions and, therefore, yields less ambiguous mobility information. In an isotropic ensemble of $^{13}CH_2$ systems, ^{1}H−^{13}C cross-relaxation is given by[14]

$$\sigma_{CH} = \frac{n}{20}\omega_{CH}^2\{6J(\omega_H + \omega_C) - J(\omega_H - \omega_C)\} \qquad (1)$$

with $n = 2$ as the number of methylene protons, $\omega_{CH} = (\mu_0/4\pi)\hbar\gamma_H\gamma_C r_{CH}^{-3} \approx 2\pi \times 21$ kHz as the ^{13}C−^{1}H dipolar coupling constant, r_{CH} as the carbon−proton distance, γ_C,γ_H as the gyromagnetic ratios, and ω_H, ω_C as the Larmor frequencies for ^{1}H and ^{13}C, respectively. The spectral density function $J(\omega)$ reflects the mobility of the internuclear CH vectors r_{CH} at frequency ω. Since ω_{CH} is inversely proportional to $1/r_{CH}^3$, the contribution by other protons outside the methylene group to the initial relaxation rate is negligible, and the $^{13}CH_2$ system is fairly isolated.

The spectral density function $J(\omega)$ represents the link between the observed NMR relaxation and the underlying rotational mobility. It can be either computed from molecular-dynamics simulations or derived from analytical models. In Lipari and Szabo's (LS) phenomenological "model-free" analysis, which is widely applied in the NMR studies of (bio)organic molecules with many degrees of rotational freedom,[11] it is assumed that the spectral density function $J(\omega)$ for a general combination of intramolecular motions and isotropic overall tumbling can be described as

$$J(\omega) = (1 - S^2)\frac{2\tau_d}{1 + \omega^2\tau_d^2} + S^2\frac{2\tau_c}{1 + \omega^2\tau_c^2} \qquad (2)$$

whereby the generalized order parameter S reflects the degree of spatial restriction of the internal motion, and $\tau_d^{-1} = \tau_e^{-1} + \tau_c^{-1}$, the combined correlation time of the effective correlation time for internal motion, τ_e, and the correlation time of the overall tumbling, τ_c. This may be substituted into eq 1 to obtain the initial cross-relaxation rate as a function of the correlation times τ_e and τ_c.

If the internal motion is extremely fast ($\omega\tau_e \ll 1$), and the overall motion is in the Larmor frequency range ($\omega\tau_c \approx 1$), the first term on the right-hand side of eq 2 can be neglected and $J(\omega)$ is dominated by the overall rotation. The internal motion has only an indirect scaling effect by partly preaveraging the ^{13}CH coupling. Inserting the second term on the right-hand side of eq 2 into eq 1, we obtain

$$\sigma_{CH} = \frac{n}{20}\frac{\omega_{CH}^2}{\omega_H}S^2\left\{\frac{12\theta}{1 + (1 + \gamma_C/\gamma_H)^2\theta^2} - \frac{2\theta}{1 + (1 - \gamma_C/\gamma_H)^2\theta^2}\right\} \qquad (3)$$

with $\theta = \omega_H\tau_c$ as the relative correlation time on the Larmor time scale and γ_C/γ_H as a field-independent constant equal to 0.25. The initial cross-relaxation rate after a perfect proton inversion (scaled to the ^{13}C equilibrium polarization at the corresponding temperature) equals $2\sigma_{CH}\gamma_H/\gamma_C \approx 8\sigma_{CH}$. Equation 3 predicts two limiting ranges. In the extreme narrowing case, $\theta \ll 1$, σ_{CH} is approximately proportional to θ, whereas, for $\theta \gg 1$, it is inversely proportional to θ. At $\theta = 0.7$, there is a maximum $\sigma_{max} = 0.37\omega_{CH}^2S^2/\omega_H$. Note the inverse proportionality to the magnetic field $B_0 = \omega_H/\gamma_H$. Equation 3 can be inverted to map the observed cross-relaxation rates directly on effective correlation times τ_c. For simplicity, we use the approximate mapping function:

$$\tau_c = \frac{\sigma_{max} \pm \sqrt{\sigma_{max}^2 - \sigma_{CH}^2}}{\sigma_{CH}}\frac{1}{\mu\omega_H} \qquad (4)$$

The parameter $\mu \approx 1.4$ is based on a local approximation of eq 3 at $\theta = 0.7$ by the function $\sigma_{max}2\mu\theta/(1 + \mu^2\theta^2)$ and is approximately valid for the range $0.01 < \theta < 3$. The sign in eq

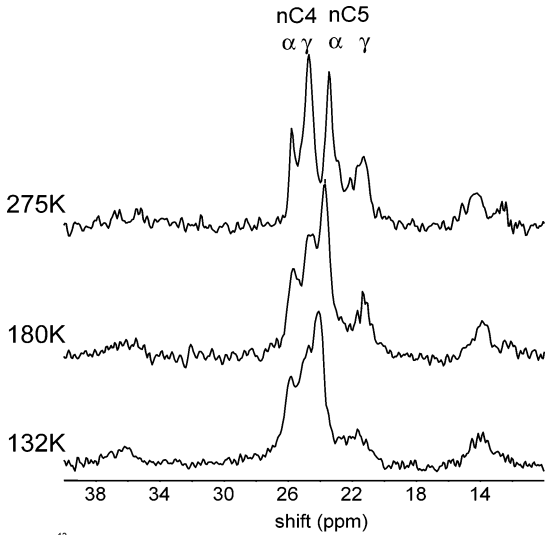

Figure 2. ^{13}C MAS NMR spectrum of a mixture of pentane (*n*C5) and butane (*n*C4) in H-ZK5 (field 11.7 T). The four methylene signals between 20 and 28 ppm represent each of the two alkanes in each of the two cage types (α and γ). Up to ~370 K (not shown), the peaks are well resolved indicating that molecular exchange between the cages is slow on the millisecond time scale.

4 depends on the size of τ_c^{-1} relative to $\mu\omega_H$. This can usually be determined from the temperature trend. If σ_{CH} increases upon a small temperature decrease, the ensemble is in the extreme narrowing limit, and the minus sign applies. If σ_{CH} decreases at decreasing temperature, $\pm$ should be replaced by $+$. It should be kept in mind that the mapping function (eq 4) is derived from eq 3 involving just the second term on the right-hand side of eq 2 and is therefore valid only if the direct influence of internal motions on the relaxation is negligible.

Experimental Section

Pentane/butane-loaded ZK-5 samples were prepared as previously described.[2] The NMR sample contained 30 mg of H-ZK-5 (Si/Al = 3.8) saturated with a mixture of 98% pentane (5% ^{13}C-labeled at C2) and 2% butane (200%-labeled at C2,3) in a sealed ampule.

^{13}C NMR experiments were carried out on a Bruker DMX500 and a Bruker MSL200 spectrometer operating at respective ^{13}C resonance frequencies of 125 and 50 MHz. The adamantane peak at 38.56 ppm was used as an external reference for the chemical shift. Magic-angle spinning (MAS) was employed to eliminate the line broadening caused by the small chemical shift anisotropy of ^{13}C nuclei in *n*-pentane. The sample rotation rate 1.5 kHz was high enough to remove spinning sidebands from the MAS spectrum and, at the same time, was sufficiently low for stable spinning of the 7-mm rotors containing the sealed glass capsules with the *n*-alkanes-loaded zeolites. For quantitative spectra (Figure 2) direct ^{13}C excitation with a single 90° pulse of 5 μs was combined with high-power proton decoupling and relaxation delays of 20 s between subsequent scans. Typically 1024 to 4096 scans were recorded. ^{1}H MAS spectra were recorded at 11.7 T using a 90° pulse of 5 μs and a sample rotation rate of 2 kHz. Two-dimensional ^{1}H−^{13}C correlation experiments were based on the wide-line-separation (WISE) technique[15] modified with Lee−Goldburg proton irradiation during the ^{1}H−^{13}C cross-polarization interval to suppress ^{1}H−^{1}H spin diffusion.[16]

^{1}H−^{13}C cross-relaxation was measured with a 180(^{1}H)−τ−90(^{13}C) pulse sequence combined with MAS and proton-decoupling during the acquisition. The resulting transient cross-relaxation curves as a function of τ were fit with a biexponent $A + B\{\exp(-\lambda_1\tau) - \exp(-\lambda_2\tau)\}$. The cross-relaxation coefficient σ_{CH} was derived from the scaled initial cross-relaxation rate as $(\lambda_2 - \lambda_1)(B/A)(\gamma_C/2\gamma_H)$, where γ_C and γ_H are the gyromagnetic ratios of ^{13}C and ^{1}H ($\gamma_H/\gamma_C \approx 4$), and the factor 2 arises from the proton inversion at time $t = 0$.

The temperature was set with the standard Bruker variable-temperature control unit, which uses a thermocouple in the N_2 bearing surrounding the spinning sample holder. A linear correction formula was obtained for the systematic difference between the indicated and the true temperature by a careful calibration based on the melting of a series of alkanes (C5−C18) as measured by ^{1}H NMR. The consistent Arrhenius dependence of the NOE, which we observe for liquid pentane below 200 K down to its freezing point (143K), serves as an additional proof of our temperature calibration.

Analysis of MAS ^{1}H NMR sideband patterns was carried out with the program WinFit from Bruker. Peak heights in transient NOE experiments at 4.7 T and 11.7 T (the latter in duplo) were collected using the standard peak picking routines in the Bruker programs 1D-WinNMR and XWinNMR, respectively. Using Microsoft Excel, we fitted biexponential curves $I(\tau) = I(0) + A\{\exp(-\lambda_1\tau) - \exp(-\lambda_2\tau)\}$ to the transient ^{1}H−^{13}C NOE curves and extracted the cross-relaxation coefficient σ as $0.5A(\lambda_2 - \lambda_1)\gamma_C/\gamma_H = A(\lambda_2 - \lambda_1)/8$. Mathematica was used to interpret the obtained cross-relaxation rates, effective correlation times, and activation energies as a function of temperature in terms of the three models discussed in this paper, as well as to estimate the error in the fit parameters. Linear models were fitted by a linear least-squares method. For all nonlinear models, a Levenberg−Marquardt method was employed inside Mathematica.

Results

At and below room temperature, the magic-angle-spinning (MAS) ^{13}C NMR spectrum of a mixture of C2-labeled pentane and C2,3-labeled butane on zeolite ZK-5 contains four resolved $^{13}CH_2$ resonances at both 4.7 and 11.7 T (Figure 2). On the basis of previous work,[2] the resonances at 25.8 and 24.7 ppm are assigned to the C2 and C3 position in butane in the α and γ cage, respectively, and those at 23.5 and 21.3 ppm are assigned to the C2 position in pentane in the α and γ cage. Around 14 ppm, the natural-abundance ^{13}C signal of the pentane methyl groups is visible. The intensities of the four major peaks reflect the comparable ^{13}C-isotope concentrations for butane and pentane. The frequency separation between the $^{13}CH_2$ signals of butane and pentane in the α and γ cages is in the order of 1 ppm, which at 4.7 T corresponds to 50 Hz. The fact that these signals are well resolved demonstrates that exchange between the two types of cages is slow on the time scale of milliseconds. Because alkane translation in ZK-5 involves an alternating pathway between α and γ cages,[3] this indicates that the residence time of the molecules in the cages is long on this time scale. In fact, in our previous work, it was shown that translational motion by intercage hopping of pentane in ZK-5 occurs at a time scale of 10 ms or longer depending on the temperature and the loading.[3] Below 180 K, a broadening of the resonance of butane and pentane in the γ cage is observed (Figure 2). This could reflect heterogeneity between the various binding states inside the cages, which at higher temperatures is averaged by the molecular intracage motion.

MAS ^{1}H NMR spectra of the pentane/butane mixture on ZK-5 are shown in Figure 3. Unlike in the ^{13}C NMR spectra, the butane contribution to the ^{1}H NMR spectra is only ca. 2% and,

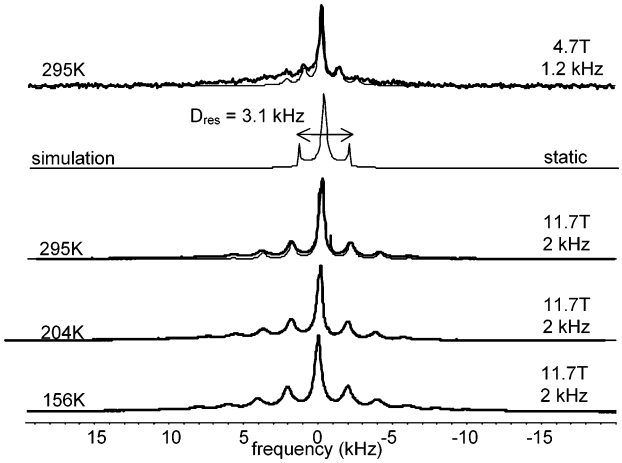

Figure 3. MAS ^{1}H NMR of the pentane/butane mixture on H-ZK5, mainly reflecting the pentane protons. The sideband pattern at the relatively low sample rotation rate of 1.2 kHz at 4.7 T (upper) and 2 kHz at 11.7 T (lower three) is indicative of strong motional averaging of the ^{1}H NMR line shape by large amplitude motions, even at 156 K. The room-temperature spectra at both fields can be described by the same combination of a Lorentzian line and the dipolar sideband pattern of a spin-$^1/_2$ pair with a residual coupling constant of ~3 kHz (simulation curves represented by thin lines in upper three spectra). At decreasing temperature, the relative intensities of the center- and sidebands do not change drastically, which means that the motional amplitudes are practically constant.

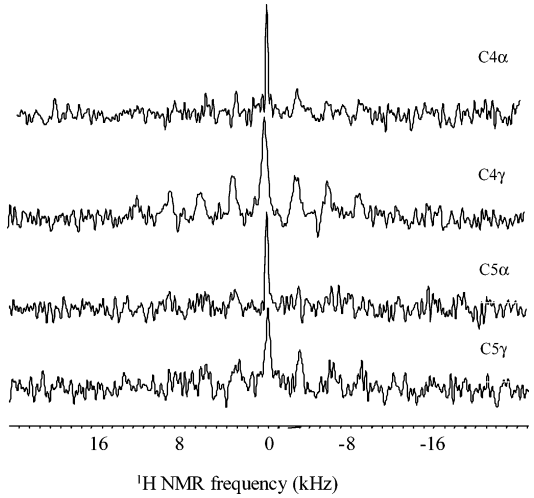

Figure 4. Separate ^{1}H NMR spectra of each type of alkanes (C4/C5) in each of the two types of cages (α/γ) in H-ZK5. The spectra were obtained as traces from a two-dimensional ^{1}H−^{13}C wide-line separation (WISE) spectrum. The sideband intensities reflect the motional amplitude. Molecular motion of both butane and pentane inside the α cages is practically isotropic, whereas motion within the γ cages is more restricted. Butane in the γ cage is particularly restrained, which is surprising, because it is smaller than pentane.

therefore, negligible. The central ^{1}H NMR line width is 0.5 kHz, independent of the magnetic field. This differs from the field-dependent, smaller line width observed for butene in the supercages of NaX, which has been explained by a combination of susceptibility and sorbate motion.[17] The sample-rotation sidebands at MAS rates as low as 1.2 kHz at 4.7 T and 2 kHz at 11.7 T are relatively weak. This indicates that the dipolar ^{1}H−^{1}H interactions in the pentane molecules are strongly reduced by large amplitude motions with short correlation times at the ^{1}H−^{1}H dipolar time scale, $\tau_c < 10^{-4}$ s. Motions at the sample-rotation time scale, $\tau_c \approx 10^{-3}$ s, would yield strong linebroadening,[18] which is not observed. For still slower motion, the MAS spectrum would extend over the 30-kz frequency range typically found for polymers in the glass or crystalline state.[19]

We have considered two possible mechanisms for the residual sideband patterns at 4.7 and 11.7 T: susceptibility broadening and incomplete motional averaging of the dipolar ^{1}H−^{1}H interactions. The two mechanisms can be discriminated by their dependence on the magnetic field. The first-order susceptibility effect on the sideband intensities, expressed as a static line width in kHz, should increase linearly with the magnetic field, whereas first-order effects of residual dipolar interactions should be field independent. To test the latter hypothesis, we employ an approach similar to the pseudo-static line shape description of ^{2}H line shapes of deuterated molecules in lipid membranes and other liquid-crystalline systems.[20,21] As follows from the rotatonial properties of second-rank tensors, fast alkane rotation about the molecular axis averages the static dipolar ^{1}H−^{1}H interaction by a factor $P_2(\cos\theta_1) = (3\cos^2\theta_1 - 1)/2$ with θ_1 as the angle between the ^{1}H−^{1}H vector and the molecular axis. Likewise, a combination of fast rotation modes leads to multiple scaling, $T = \Pi P_2(\cos\theta_k)$ with θ_k, for $k > 1$, as the angle between subsequent rotation axes. Magic-angle spinning splits the motionally (pre-)averaged dipolar line shape into a sideband pattern with intensities reflecting the residual dipole coupling constant $D_{res} = TD_{HH}$ with D_{HH} as the static coupling constant, typically 22 kHz for proton−proton interactions in methyl and methylene moieties. Analysis of the room-temperature MAS ^{1}H NMR spectra at 4.7 and 11.7 T reveals that both are well described by the same combination of a Lorentzian (40%; $T = 0$) and the dipolar sideband pattern of a spin-$^1/_2$ pair $D_{res} = 3.1$ kHz (60%; $T = 0.14$). The field independence of the fit parameters indicates that residual dipolar coupling, rather than susceptibility, dominates the MAS ^{1}H NMR sideband patterns. Between 160 K and 300 K, there is little influence of the temperature on the relative sideband intensities compared to the centerband. This indicates that the weak amplitude restrictions on the rotational motion are fairly temperature constant.

For a detailed insight into the motional anisotropy of butane and pentane in each of the two cage types, we have carried out a two-dimensional ^{1}H−^{13}C Wide-line separation (WISE) experiment[15] with suppressed ^{1}H−^{1}H spin diffusion. This experiment combines the mobility information in the ^{1}H dimension with the resolution along the ^{13}C frequency axis and, thus, yields insight into the alkane mobility in the α and γ cages separately. The ^{1}H traces taken from the WISE spectrum at the four respective ^{13}C shift positions (Figure 4) are indicative of a practically isotropic mobility of butane and pentane in the α cages and a slightly more restricted type of motion of the alkanes in the γ cages. Surprisingly, butane inside the γ cage appears to be more restricted than pentane, although the latter has a larger molecular size.

To study the motional time scale we have carried out a temperature study of ^{1}H−^{13}C cross-relaxation at two different magnetic fields, 4.7 and 11.7 T. Like the MAS ^{1}H NMR spectra, the extensive ^{1}H−^{13}C cross-relaxation indicates that pentane in the zeolite cages between 143 and 180 K are not in a completely immobilized state. For example, for solid pentane below the freezing point 143 K, no measurable NOE occurs. As illustrated in Figure 5, a similar general trend is observed in the Arrhenius plots for each alkane in each of the two cage types. The initial cross-relaxation rates show a clear Arrhenius behavior above 200 K, whereas below 180 K the rates are fairly constant down to 140 K. Although the general trend is similar, there are individual differences, indicating that the rotational dynamics of pentane and butane in each of the two cage types is not the same.

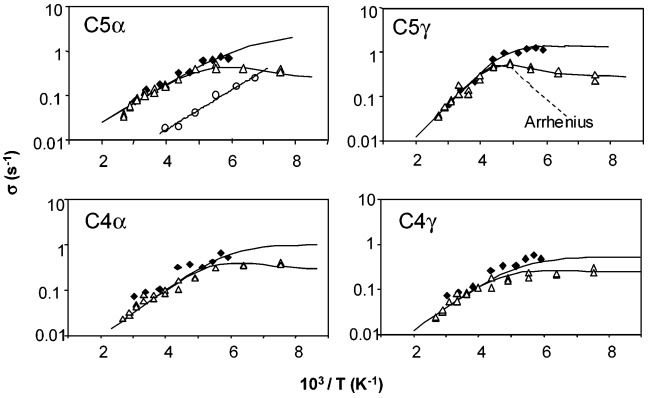

Figure 5. Arrhenius plot of $^1H-^{13}C$ cross-relaxation coefficients σ_{CH} for pentane (C5) and butane (C4) in the α and γ cage of zeolite ZK-5 at a magnetic field of 4.7 T (◆) and 11.7 T (△). The curves shown are drawn on the basis of a bicomponent fit of activated and nonactivated motion (Model A) with parameters indicated in Table 3 (Appendix 2). Equation 3 was used to compute the corresponding curves at 4.7 and 11.7 T. For comparison, the upper left part also contains the cross-relaxation rates observed for liquid pentane at 11.7 T down to its freezing point at 143 K (upper left). In the upper-right figure, a standard log-hyperbolic (Λ shaped) curve for activated motion characterized by a single correlation time has been illustrated (broken line).

Discussion

A. General Interpretation in Terms of Lipari and Szabo's Model-Free Approach. If $^1H-^{13}C$ cross-relaxation would be caused by activated motion characterized by a single correlation time $\tau = \tau_0 \exp(E_A/RT)$, the relaxation rates would present a typical log-hyperbolic (symmetric "Λ") shape in Arrhenius plots.[22] Obviously, the temperature dependence $^1H-^{13}C$ cross-relaxation of butane and pentane inside the α and γ cages deviates from such a standard log-hyperbolic curve (Figure 5). The simplest form of Lipari and Szabo's (LS) approach (eq 2) with internal and overall motion characterized by single correlation times $\tau_e = \tau_{e0} \exp(E_a/RT)$ and $\tau_c = \tau_{c0} \exp(E_c/RT)$ cannot explain the observed temperature behavior either. Around 200 K there is a transition from a strong to weak temperature dependence. This suggests a combination, $\tau_d^{-1} = \tau_e^{-1} + \tau_c^{-1}$, like in the first term of the Lipari−Szabo (LS) spectral density function (eq 2), of activated internal motion and nonactivated overall motion, or vice versa, with both $\omega_H\tau_e$ and $\omega_H\tau_c$ in the order of 1 at 200 K. However, the two terms in the LS approach are coupled by the order parameter S and overall tumbling time τ_c and cannot be varied independently. For a good description of the observed temperature transition by an activated and a nonactivated component, the first term should dominate the temperature dependence. However, the maximum cross-relaxation coefficients predicted for $S = 0$, i.e., 2 s^{-1} at 11.7 T, exceed the observed values by a factor of 4−5 (Figure 5). Increasing S^2 to ∼0.8 in order to explain the lower relaxation maximum is no option, because this would make the second term of the LS model too prominent. The second term only depends on τ_c and therefore cannot explain the observed transition from activated to nonactivated motion, unless the overall tumbling itself has a non-Arrhenius temperature dependence.

As the next simplest model, let us, therefore, consider a combination of extremely fast internal motion ($\omega_H\tau_e \ll 1$) and a non-Arrhenius type of overall tumbling in the Larmor frequency range ($\omega_H\tau_c \approx 1$). The first could represent fast uniaxial rotation of the methylene CH vectors caused by alkane motion about the molecular axis, perhaps with a contribution by C−C bond rotation. The second could be the overall tumbling of the molecular axis itself, which would typically be isotropic in the α cage but anisotropic in the γ cage due to steric constraints. The motional narrowing of the $^1H-^1H$ dipolar coupling observed in the ^1H NMR spectra (Figure 3) and the ^1H traces from the WISE spectra (Figure 4) support such a picture. In the all-trans conformation, the methylene CH vectors are perpendicular to the molecular axis, and extremely fast uniaxial motion about this axis would lead to a prescaling of the $^{13}C-^1H$ dipolar interaction by an order parameter of $S = {}^1/_2$. The resulting NMR relaxation caused by the isotropic overall tumbling of the molecular axis in the α cage is then expected to be scaled by a factor of $S^2 = {}^1/_4$. Indeed, we extract S^2 values between 0.2 and 0.3 from the observed cross-relaxation maxima at 11.7 T (Figure 5; Table 1 in Appendix 2) using the theoretical value $\sigma_{max} = 0.37S^2\omega_{CH}^2/\omega_H = 2.0\ S^2\ s^{-1}$ numerically derived from eq 3.

The ^1H NMR spectra (Figures 3 and 4) reflect slightly anisotropic overall motion of butane and pentane in the γ cages. The oblate cage shape forces a residual orientational order on the encapsulated alkane molecule. As compared to isotropic overall motion, the residual order scales the initial powder-average $^1H-^{13}C$ cross-relaxation after a proton inversion by a factor of $1 - T^2$, where T denotes an effective order parameter reflecting the scaling of the $^1H-^{13}C$ interaction (Appendix 1). Since $^1H-^{13}C$ cross-relaxation is mainly sensitive to motions in the Larmor range ($10^{-10}-10^{-8}$ s), we neglect the influence of the sample rotation (10^{-3} s). More precisely, the spectral density $J(\omega)$ should be fairly constant over a range of a few kHz around the frequencies $\omega_H \pm \omega_C$.[13] In the all-trans conformation, the methylene HH and CH vectors are perpendicular to the molecular axis ($\theta_1 = \pi/2$), and by further assumption, the molecular axis of butane and pentane in the γ cage is always within the equatorial plane perpendicular to the cage C_4 axis ($\theta_2 = \pi/2$). Then, biaxial rotation of the CH_2 groups about the molecular axis ($\omega\tau_e \ll 1$) and the major axis of the γ cage ($\omega\tau_c \approx 1$) should scale the dipolar $^1H-^1H$ coupling by $T = P_2(\cos\theta_1)P_2(\cos\theta_2) = {}^1/_4$, and the initial cross-relaxation by $S^2(1 - T^2) = {}^{15}/_{64} \approx 0.23$ (Appendix 1). This is reasonably consistent with the value $T = 0.14$ extracted from the observed motional narrowing of the MAS ^1H NMR sideband pattern (Figure 3) and agrees well with the ratios between the observed σ_{max} values at 11.7 T and the maximally possible value 2.0 s^{-1} at this field (Table 1, Appendix 2). Below a certain degree of anisotropy, $T < 0.3$, the cross-relaxation is practically the same as for isotropic overall motion.

The observed cross-relaxation rates can be mapped onto effective rotation correlation times using eq 4 with the σ_{max} values indicated in Table 1 (Appendix 2). For pentane, σ_{max} satisfies the expected inverse proportionality to the magnetic field, and the effective correlation times τ_c resulting from independent measurements at 4.7 and 11.7T consistently fall onto a single curve with a non-Arrhenius type of temperature dependence (Figure 6). The consistent description of $^1H-^{13}C$ cross-relaxation at 4.7 and 11.7 T by eq 4 supports the validity of standard relaxation theory for pentane in ZK-5.

For butane, the situation is more complicated, because cross-relaxation at 4.7 T tends to be systematically faster than expected from the data measured at 11.7 T and the inverse-field proportionality factor 2.5 (Figure 5). In fact, we must take σ_{max} at 4.7 T 4 to 5 times bigger than at 11.7 T to let the tumbling times derived from the data at the two fields coincide (Figure 6). A strongly enhanced relaxation at decreasing magnetic field indicates a possible role of homonuclear $^1H-^1H$ or $^{13}C-^{13}C$ spin diffusion as one of the steps in a relayed type of cross-

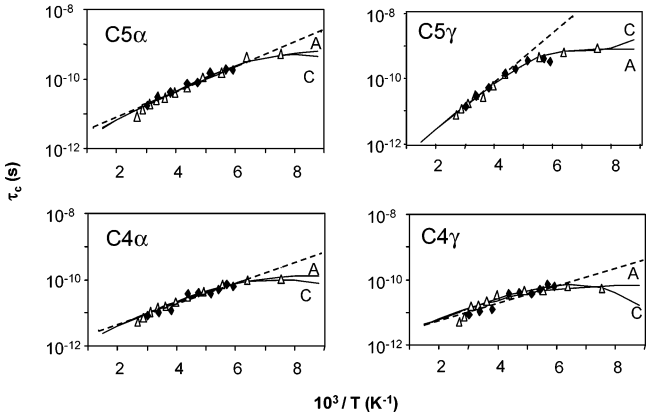

Figure 6. Arrhenius plot of effective tumbling times τ_c for pentane (C5) and butane (C4) in the α and γ cage at 4.7 T (◆) and 11.7 T (△) derived from the experimental σ_{CH} values (Figure 5) according to eq 5. The deviation from Arrhenius behavior, indicated by broken lines with parameters given in Table 2 (Appendix 2), is obvious. The continuous curves correspond to respective fits of Models A and C with parameters indicated in Tables 3 and 5 (Appendix 2).

relaxation $^1H \rightarrow {}^1H \rightarrow {}^{13}C$ or $^1H \rightarrow {}^{13}C \rightarrow {}^{13}C$. Spin diffusion between alike nuclei is inversely proportional to the square of the field.[19] Theoretically, spin diffusion should not affect the initial slope, since at $t = 0$ all ^{13}C nuclei are still in thermal equilibrium. In practice, however, a finite-difference quotient, rather than a true derivative at $t = 0$ is determined. If the intrinsic cross-relaxation is slow enough, the initial slope may become contaminated by $^{13}C-{}^{13}C$ or $^1H-{}^1H$ spin diffusion, for example, similar to proton spin−lattice relaxation in polymer blends.[19] The question why cross-relaxation for butane at 4.7 T would be more affected by spin diffusion than pentane puzzles us. The fact that butane in our experiments was doubly ^{13}C-labeled at adjacent methylene positions may be part of an explanation.

In summary, the observed relaxation as a function of temperature indicates an anisotropic ultrafast internal motion combined with a fairly unrestricted non-Arrhenius type of overall motion. Equations 3 and 4 offer a consistent explanation for pentane at 4.7 and 11.7 T in terms of a single, effective correlation time, which we associate with the overall motion. For butane an additional scaling factor (∼2), perhaps associated with spin diffusion, has to be invoked to explain the strong field dependence. The reason for the non-Arrhenius behavior of the overall motion is not obvious, and we have considered various possible explanations.

B. Model A: Activated and Nonactivated Rotational Pathways inside the Zeolite Cages. Phenomenologically the temperature dependence of the effective rotational correlation time is well-described by a combination of activated and nonactivated rotation with an effective correlation time τ_c given by

$$\frac{1}{\tau_c} = \frac{1}{\tau_{a0}\exp(E_a/k_BT)} + \frac{1}{\tau_{na}} \qquad (5)$$

Equation 5 is similar to the definition of τ_d in the Lipari−Szabo model (eq 3b), which represents a combination of internal and overall motion. However, we have already assumed τ_d to be ultrashort to explain the relatively low σ_{max} values at 11.7 T, combined with the extensive motional averaging of the ^1H NMR line shapes. Equation 5 concerns an additional splitting of the correlation time τ_c for overall motion, into an activated and nonactivated component. The model offers a consistent explanation of the cross-relaxation data for pentane (Figure 5) and the effective correlation times extracted by use of eq 4 (Figure 6). A reasonable coupled fit to the butane relaxation data at both fields is possible. However, even the "best" fit shows a systematic deviation from the experimental data as a result of the stronger field dependence than that expected from eq 3. By use of the additional scaling factor mentioned above, the butane data at 4.7 and 11.7 T can be mapped onto a consistent set of correlation times, which is well described by eq 4.

The apparent activation energies estimated with this model are in the range 6−14 kJ/mol (Appendix 2, Table 3). These values are between the typical barriers of 12−15 kJ/mol for C−C bond rotation in alkanes and the activation energies of ca. 6 kJ/mol, which can be estimated from the temperature-dependent viscosity of butane and pentane tabulated elsewhere.[23] NMR cross-relaxation measurements in liquid pentane yield an activation energy of ∼8 kJ/mol for the overall rotation (Figure 5). A rough computation of the van der Waals energy of (all-trans) pentane inside the γ cage yields barriers of 15 kJ/mol for rotation of the molecular axis about the C_4 symmetry axis of the cage.[24] Note that, unlike the α cage, the γ cage can contain no more than a single molecule, so that sorbate−sorbate interactions can be neglected. Typical activation energies in the order of 5−12 kJ/mol are also predicted from self-diffusion of short *n*-alkanes in silicalite.[25] This confirms our interpretation that the observed NMR relaxation mainly reflects the overall tumbling of the short alkane molecules inside the zeolite cages. The pre-exponential factors τ_{a0} of the activated components are close to the standard value 10^{-13} s of transition-state theory. For the respective nonactivated components, temperature-constant correlation times τ_{na} in the range $10^{-10}-10^{-9}$ s are estimated. This happens to correspond to the condition $\omega_H\tau_c \approx 1$ at which cross-relaxation has its maximum. In a way this is surprising, because there is no a priori reason, the molecular rotation would be somehow coupled to its NMR properties.

Although a combination of activated and nonactivated overall motion offers a good phenomenological description, the nature of the nonactivated component τ_{na} is unclear. It could perhaps represent some entropicly unfavorable rotational pathway without energy barriers. However, despite a strong effort to compute the van der Waals energy of butane and pentane in the γ cage (the situation in the α cage would be complicated by the presence of sorbate−sorbate interactions), we were unable to find indications for such smooth rotation pathways. Quantum tunnelling is not a realistic option because of the high-temperature range, 160−200 K, in which the transition from highly to less activated motion occurs. Methyl rotation with an activation barrier 4 kJ/mol and a moment of inertia 10^{-47} kg m^2 shows a transition from the thermal to the quantum regime around ∼10 K.[25] For the heavier pentane (10^{-45} kg m^2), rotational tunneling should be dominant only below 0.1 K. Due to the narrow windows between the cages, translational intercage diffusion of butane and pentane is too slow to affect $^1H-{}^{13}C$ cross-relaxation.[3]

C. Model B: Correlation Time Distribution. Arrhenius plots of NMR relaxation observed for alkane waxes and polymers tend to deviate from a symmetric log-hyperbolic shape due to heterogeneity effects. A log-Gaussian distribution of rotational correlation times, as well as other distribution functions, has been proposed for this purpose.[19] If the pre-exponential factor τ_{c0} and activation energy E_a are statistically independent and the latter has a Gaussian distribution $\exp[-(E_a - \langle E_a\rangle)^2/W^2]$ with negligible density at $E_A = 0$ ($3W < \langle E_a\rangle$),

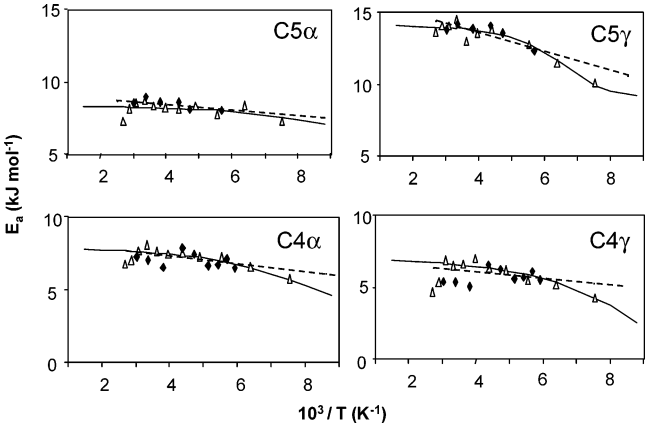

Figure 7. Arrhenius plot of effective activation energy E_a for pentane (C5) and butane (C4) in the α and γ cage at 4.7 T (◆) and 11.7 T (△) derived from effective correlation times τ_{eff} (Figure 6) combined with pre-exponential factors estimated from Model A. According to Model B, a Gaussian distribution of activation energies results in a linear decay of E_a as a function of $1/T$ (broken line; Table 4 (Appendix 2)). The continuous curve corresponds to a fit of Model C with parameters identical to those in Figure 6.

the average residence time equals

$$\langle\tau_c\rangle = \langle\tau_{c0}\rangle\exp\left(\frac{\langle E_a\rangle}{RT} - \frac{W^2}{(2RT)^2}\right) = \langle\tau_0\rangle\exp\left(\frac{E_{eff}(T)}{RT}\right) \quad (6)$$

with apparent activation energy $E_{eff}(T) = \langle E_a\rangle - W^2/4RT$.

By use of the pre-exponential factors τ_{c0} extracted from the high-temperature regime (equal to τ_{a0} of Model A), the effective correlation times (Figure 6) can be further mapped onto effective activation energies $E_{eff} = R\ \ln(\tau_{eff}/\tau_{c0})$. If the highest- and lowest-temperature data are neglected, a linear decrease of $E_{eff}(T)$ as a function of inverse temperature $1/T$ reasonably fits the extracted activation energies, indeed (Figure 7). The highest value of $\langle E_a\rangle$ is found for pentane in the γ cage (17 kJ mol^{-1}), which reflects the molecular constrainment of pentane inside this cage. For pentane in the α cage and butane in both cages, lower values between 9 and 10 kJ mol^{-1} are obtained (Appendix 2, Table 4). As for the distribution widths W, the lowest value (2.7 kJ mol^{-1}) is found for pentane in the α cage, while the other widths are ca. 4 kJ mol^{-1}. This is counterintuitive, because we expect more heterogeneity for the α cage given its various loading states (0−3 molecules per cage). If, indeed, the deviation from the symmetric log-hyperbolic shape in the Arrenius plot of cross-relaxation is a measure of heterogeneity, how can the motional heterogeneity in the crystalline zeolites be even bigger than in amorphous alkane waxes, with their more symmetric relaxation plots?[27] An explanation could be small lattice distortions associated with a random positioning of Al atoms in the zeolite lattice. Indeed, given the Al content of ZK-5 (Si/Al = 3.8), a large number of different Al substitutions are statistically possible. Whether or not the Al atoms are actually randomly positioned in the lattice, however, is a matter of scientific debate. The well-defined crystal structure obtained from XRD studies seems to exclude significant distortions of the regular crystal structure as a source of heterogeneity.

D. Model C: Collective Sorbate−Lattice Motion. As an alternative cause of nonactivated motion we have looked into the influence of lattice flexibility. A number of groups have studied the effect of phonon coupling and lattice flexibility on Brownian motion by molecular simulation.[28−32] Sorbate−zeolite interactions can be strong enough to induce significant changes in the lattice structure as big as crystal phase transitions.[33,34] A molecule inside the zeolite cavity does not only *passively* respond to van der Waals and Coulomb forces generated by the lattice atoms and extra-lattice cations but also *actively* exerts a force on the lattice atoms, which, depending on the lattice flexibility, respond by small structure deformations. Our computation of the van der Waals energy suggest that the oblate shape of the γ cage restricts the molecular-axis motion of butane and pentane to in-plane rotation perpendicular to the cage C_4 axis.[24] Within the cage plane, the molecular axis has four stable orientations separated by energy barriers. Interestingly, a small longitudinal cage expansion lowers both the energy of the stable and metastable orientations, although the latter substantially more than the first. When a butane or pentane molecule resides in a stable orientation site sufficiently long at the lattice-deformation time scale, this causes a local expansion of the cage and simultaneously lowers the barrier for a rotational jump to the adjacent site. On the basis of this picture, we have recently developed a statistical mechanical model for sorbate motion in a deformable lattice and discovered a remarkable transition at the onset of concerted sorbate−lattice motions.[24] In our model, the interactions between the adsorbed alkane molecule and overdamped local lattice-deformation modes are represented up to second-order in the mode coordinates q_k by the sorbate−phonon coupling term:

$$H_{int} = \sum_k^N W^{(1)}(\phi)q_k + \frac{1}{2}W^{(2)}(\phi){q_k}^2 \quad (7)$$

where $W^{(1)}(\phi)$ and $W^{(2)}(\phi)$ are $\pi/2$-periodic functions of the molecular-axis orientation in the cage plane. For a constant phonon density $g(\omega) = 1/\omega_{max}$ with frequencies between 0 and ω_{max}, which describes the experimental vibration spectra of zeolites better than, e.g., the common Debye phonon density,[35] our model predicts an effective energy barrier given by[24]

$$\Delta V_{eff} = \Delta V - \frac{U}{\omega_{max}\omega_c}\arctan\left(\frac{\omega_{max}}{\omega_c}\right) \quad (8)$$

Here ΔV denotes the energy barrier in the absence of lattice deformation, and U is a measure for the difference in the linear sorbate−phonon coupling at the binding sites and at the barriers. The effective frequency

$$\omega_c = \sqrt{{\omega_2}^2 + \gamma{\tau_{c0}}^{-1}e^{-E_{aa}/RT}} \quad (9)$$

is related to the phonon damping coefficient γ, assumed frequency-independent, and the sorbate-residence time at the binding sites $\tau_c \approx \tau_{c0}\ \exp(E_a/RT)$, approximately taken as in the rigid lattice. The parameter ω_2 arises from sorbate−phonon coupling terms which are quadratic in the phonon coordinates and represents an effective lower bound frequency preventing the lattice from a complete collapse in the limit $\tau_c \rightarrow \infty$. If $\omega_{max} \gg \omega_2$ and $\gamma{\tau_{c0}}^{-1} > {\omega_2}^2$, the models predict a sigmoid decrease of ΔV_{eff} as a function of inverse temperature from ΔV at high temperature ($T \rightarrow \infty$) to $\Delta V - (\pi/2)U/\omega_{max}\omega_2$ at low temperature ($T \rightarrow 0$). The halfway value is reached at temperature $T^* = \Delta V/|R\ \ln(0.33{\omega_2}^2\tau_{c0}/\gamma)|$, when τ_c is equal to $\tau_{dl} \equiv 0.33\ \gamma/{\omega_2}^2$.[20] The latter may be regarded as the predominant deformation time scale of a lattice with this phonon distribution. Above T* particle motion is fast as compared to the deformation, and the particle diffuses in a quasi-rigid lattice with barriers ΔV. Below T^*, the particle position and lattice deformation are coupled, resulting in a concerted motion with a lower activation barrier.

The model explains the non-Arrhenius type of rotational motion of pentane inside zeolite ZK-5 observed with $^1H-^{13}C$ NMR relaxometry, equally well as Model A and slightly better than Model B, especially for the highest and lowest temperatures. Relevant simulation-parameter values are given in Table 5 (Appendix 2). The model involves the same pre-exponential factors τ_{c0} and rigid-barrier values ΔV as models A and B. Typical values of the two other fit parameters $\tau_{dl} \equiv 0.33\ \gamma/\omega_2^2$ and $U/\omega_{max}\omega_2$ are in the order of 10^{-9} s and 3 kJ mol^{-1}, respectively. Due to experimental limitations, we could not measure cross-relaxation below 130 K, which was insufficient to precisely determine the low-temperature limit for the activation energy. Especially for butane and pentane in the α cage, this yields relatively large inaccuracies in the fit parameters. These are thus safely regarded as simulation parameters with no other aim than to show that, at least, with these parameter values we can simulate the observed behavior.

Conclusion

In this article we have presented the results of $^1H-^{13}C$ cross-relaxation measurements of a mixture of *n*-butane and *n*-pentane on zeolite ZK-5 at 4.7 and 11.7 T. Using magic-angle-spinning (MAS) ^{13}C NMR spectroscopy, we separately detected the NMR relaxation for each alkane in each of the two ZK-5 cage types accessible for short alkanes. The observed cross-relaxation for the butane and pentane methylene moieties and ^1H spectra indicate large amplitude rotational motion. The cross-relaxation rates are consistent with ultrafast rotation about the alkane axis combined with slower tumbling of the molecular axis itself. Two temperature regimes were discovered. In the high-temperature range (200−320 K), the effective tumbling times show Arrhenius behavior with activation energies in the range 6−14 kJ/mol, as consistent with van der Waals computations. Below 200 K, however, the relaxation has weak temperature dependence. We have considered three possible models that give a good phenomenological description of the temperature dependences of overall molecular rotation: (A) a combination of activated and nonactivated motion, (B) a Gaussian distribution of activation energies, and (C) collective sorbate−zeolite motions. Models A and C yield equally good phenomenological descriptions, and Model B fits also reasonably well. However, problems arise when trying to interpret the resulting fit parameters. As for Model A, the existence of nonactivated rotational pathways is unlikely, because any theoretical consideration gives no evidence for the existence of smooth rotational pathways without barriers. As for Model B, the motional heterogeneity required to explain the non-Arrhenius behavior is unrealistically large (e.g., larger than that in amorphous waxes), given the high regularity of the pore shapes in the zeolite crystallites. Model C offers a tentative but intriguing explanation in terms of concerted sorbate−zeolite motions. By causing dynamic lattice deformations, the adsorbed molecules facilitate their own barrier crossing. More experiments, e.g., based on ^{29}Si and ^{27}Al NMR of the zeolite lattice with and without adsorbed molecules, are necessary to further test this hypothesis.

Acknowledgment. The authors gratefully acknowledge valuable contributions to this work by Arnaud Travert, Yannick Millot, and Danny Schuring.

Appendix 1. Effect of Static Components in the Dipolar Hamiltonian on NMR Relaxation

Most NMR relaxation theories do not treat the effects of static components in the dipolar Hamiltonian explicitly. The relaxation master equation is usually derived from the approximate solution of the Liouville equation under the assumption that orientation correlations vanish quickly as compared to the change of the spin density matrix.[10] Without this assumption, it can be derived in an analogous way that the ^{13}C polarization after a "homogeneous" proton inversion in all $^{13}CH_2$ systems (so that no orientation correlation between the dipolar Hamiltonian and the density matrix exists at $t = 0$) initially develops as

$$\Delta\langle I_z\rangle_t = \frac{n}{20}\omega_{CH}{}^2\Delta\langle S_z\rangle_0\int_0^t\{6J_2(\omega_H+\omega_C,t') - J_0(\omega_H-\omega_C,t')\}\,dt' \quad (A1)$$

whereby $\Delta\langle I_z\rangle_t$ and $\Delta\langle S_z\rangle_0$ denote the deviation from the ^{13}C and ^1H polarization at time t and 0, respectively, and the "incomplete" spectral density functions $J_n(\omega,t')$ are given by

$$J_n(\omega,t') = \int_0^{t'}\langle F_{-n}(\Omega_{CH}(0))F_n(\Omega_{CH}(\tau))\rangle\cos(\omega\tau)\,d\tau \quad (A2)$$

with $F_0(\ \Omega_{CH})$ and $F_{\pm2}(\Omega_{CH})$ as the orientation-dependent coefficients of the zero- and double-quantum spin operators $A_0 = I_+S_- + I_-S_+$ and $A_{\pm2} = 2I_\pm S_\pm$ in the dipolar Hamiltonian $H_D = \hbar\omega_D\ \Sigma\ F_n(\ \Omega_{CH})\ A_n$.[10] The difference with the conventional approach is, that the integration upperbound in Eq. A2 is not extended to infinity, and, as a result, $J_n(\omega,t')$ is still a function of time. The orientation Ω_{CH} of the CH dipolar tensor in the laboratory frame is most conveniently specified by a sequence of three rotation steps: first, the orientation Ω'_{CH} of the CH dipolar tensor in a coordinate frame fixed to the alkane molecule with the *z* axis along the molecular axis; then, the orientation Ω_{MF} of this molecular frame relative to a frame fixed to the γ cage with the *z* axis along the cage C_4 axis; and, finally, the orientation Ω_{CF} of this cage frame in the laboratory frame with the magnetic field along the *z* axis. For molecular rotation without conformation changes in a static zeolite powder, Ω_{MF} would be fluctuating in time, while Ω'_{CH} and Ω_{CF} would be static. In particular, for biaxial alkane motion inside the γ cage first about its molecular axis, and then about the major cage axis, $\Omega_{MF}(t)$ is of the form $(\alpha_{MF}(t), \beta_{MF}, \gamma_{MF}(t))$, where $\alpha_{MF}(t)$ and $\gamma_{MF}(t)$ undergo stochastic variations, while β_{MF} represents the fixed angle between the molecular axis and the cage axis ($\sim\pi/2$). By assumption, the methylene CH vectors in butane and pentane in the all-trans conformation are perpendicular to the molecular axis, and the molecular axis of butane and pentane in the γ cage is perpendicular to the cage C_4 axis ($\beta'_{CH} = \pi/2 = \beta_{MF}$). By use of the Wigner rotation matrix elements for second-rank tensors $D^2_{mn}(\alpha,\beta,\gamma) = \exp(in\alpha)\ d^2_{mn}(\beta)\ \exp(im\gamma)$,[36] the functions $F_n(\ \Omega_{CH}) \equiv F_n(\Omega_{CF}, \Omega_{MF}, \Omega'_{CH})$ can be written as a sum $\sqrt{(5/8\pi^2)}\ \Sigma D^2_{0m}(\Omega'_{CH})\ D^2_{mm'}(\Omega_{MF})\ D^2_{m'n}(\Omega_{CF})$ over $-2 \le m, m' \le 2$. For the biaxial rotation model, $F_n(\ \Omega_{CH})$ then contains a static term $A_n(\Omega_{CF}) = \sqrt{(5/8\pi^2)}\ T\ D^2_{0n}(\Omega_{CF})$ with order parameter $T = d^2_{00}(\beta'_{CH})\ d^2_{00}(\beta_{MF}) = {}^1/_4$. The remaining time-depending part $B_n(\Omega_{CF}, \Omega_{MF}, \Omega'_{CH}) = F_n(\Omega_{CF}, \Omega_{MF}, \Omega'_{CH}) - A_n(\Omega_{CF})$ has a vanishing time average. Note the orthogonal properties $\langle A_{-m}(\Omega_{CF})\ B_n(\Omega_{CF}, \Omega_{CH})\rangle = 0$, $\langle A_{-m}(\Omega_{CF})\ A_n(\Omega_{CF})\rangle = \delta_{mn}T^2$, and $\langle B_{-m}(\Omega_{CF},\Omega_{CH})\ B_n(\Omega_{CF},\Omega_{CH})\rangle = \delta_{mn}(1 - T^2)$. For a Lipari−Szabo type of correlation loss $\langle B_{-n}(\Omega_{CF}, \Omega_{MF}(0), \Omega_{CH})\ B_n(\Omega_{CF}, \Omega_{CH}(\tau)), \Omega_{CH})\rangle = (1 - T^2)\{(1 - S^2)\ \exp(-\tau/\tau_e) - S^2\}\ \exp(-\tau/\tau_c)$ with ultrafast internal motion $\omega\tau_e \ll 1$, eq 2 reduces at sufficiently long time scale $t \gg \tau_c$ to approximately:

$$J_n(\omega,t) = (1 - T^2)S^2\frac{2\tau_c}{1+\omega^2\tau_c{}^2} + T^2\frac{\sin(\omega t)}{\omega} \quad (A3)$$

TABLE 1: σ_{Max} Values Used for Mapping Cross-Relaxation Data on Effective Correlation Times by Use of Eq 4 (Figure 6)

	σ_{max}(11.7 T)	σ_{max}(4.7 T)	ratio
C5α	0.50 ± 0.05	1.3	2.5
C5γ	0.55 ± 0.05	1.4	2.5
C4α	0.50 ± 0. 05	2.5	5.0
C4γ	0.50 ± 0.05	2.5	5.0

TABLE 2: Activated Motion with a Single Correlation Time in the High Temperature Range (200−370 K), $\tau_c = \tau_{c0}$ exp($-E_a/RT$) (Figure 5)

	log(τ_{c0}/1 s)	E_a (kJ mol^{-1})
C5α	−11.2 ± 0.2	8.7 ± 1.0
C5γ	−12.0 ± 0.3	13.4 ± 1.5
C4α	−11.0 ± 0.2	6.5 ± 0.8
C4γ	−11.0 ± 0.27	6.2 ± 1.2

TABLE 3: Two Components (Model A), $\tau_c^{-1} = \tau_{a0}^{-1}$ exp($-E_a/RT$) + τ_{na}^{-1} (Figures 5 and 6)

	log(τ_{a0}/1 s)	E_a (kJ mol^{-1})	log(τ_{na}/1s)
C5α	−11.2 ± 0.2	8.6 ± 1.2	8.1 ± 0.3
C5γ	−12.1 ± 0.4	14.4 ± 2.2	8.2 ± 0.2
C4α	−11.4 ± 0.3	8.8 ± 1.5	8.8 ± 0.8
C4γ	−11.7 ± 0.4	10.9 ± 3.6	9.1 ± 0.1

TABLE 4: Gaussian Heterogeneity (Model B), $E_{eff}(T) = \langle E_a \rangle - W^2/4RT$ (Figure 7)

	log(τ_{c0}/1 s)	$\langle E_a \rangle$ (kJ mol^{-1})	W (kJ mol^{-1})
C5α	−11.2 ± 0.2	9.1 ± 0.6	2.7 ± 0.8
C5γ	−12.0 ± 0.3	16.9 ± 1.0	5.4 ± 0.4
C4α	−11.0 ± 0.2	10.0 ± 0.6	3.9 ± 0.5
C4γ	−11.0 ± 0.27	9.1 ± 0.9	4.1 ± 0.7

TABLE 5: Sorbate−Lattice Coupling (Model C) $\Delta V_{eff} = \Delta V - U\omega_{max}^{-1}\omega_c^{-1}$ arctan(ω_{max}/ω_c) (Figures 6 and 7)[a]

	log(τ_{ld}/1 s)	U ω_{max}^{-1} ω_2^{-1} (kJ mol^{-1})
C5α	−8.8	2.9
C5γ	−8.6 ± 0.4	2.9 ± 0.2
C4α	−9.1	3.0
C4γ	−9.4 ± 0.6	3.2 ± 0.5

[a] τ_{c0} and ΔV same as τ_{c0} and E_a for Model A (Table 3).

The first term on the right-hand side has the familiar form and causes relaxation at a steady rate proportional to $(1 - T^2)S^2/\omega$ for motion in the Larmor range, $\omega\tau_c \approx 1$. The second represents periodic second-order effects of the static, nonsecular terms in the dipolar Hamiltonian with oscillation amplitude T^2/ω. For not too small values of $(1 - T^2)S^2$, the second term quickly becomes negligible in the time integral (eq A1), and we are left with cross-relaxation scaled by a factor of $(1 - T^2)$ as compared to the case of isotropic overall motion.

Appendix 2. Parameters in the Various Models

The parameters are shown in Tables 1−5. The fit parameters are given with error bars, and the simulation parameters are given without error bars.

References and Notes

(1) Lievens, J. L.; Verduijn, J. P.; Mortier, W. J. *Zeolites* **1992**, *12*, 690.

(2) van Well, W. J. M.; Jänchen, J.; de Haan, J. W.; van Santen R. A. *J. Phys. Chem. B* **1999**, *103*, 1841.

(3) Magusin, P. C. M. M.; Schuring, D.; Van Oers, E. M.; De Haan, J. W.; Van Santen, R. A. *Magn. Reson. Chem*. **1999**, *37*, S108.

(4) Jobic, H. *Curr. Opin. Solid State Mater. Sci*. **2002**, *6*, 415.

(5) Huwe, A.; Kremer, J.; Kärger, J.; Behrens, P.; Schwieger, W.; Ihlein, G.; Wei*β*, Ö; Schüth, F. *J. Mol. Liq*. **2000**, *86*, 173.

(6) Stallmach, F.; Kaerger, J. *Adsorption* **1999**, *5*, 117.

(7) Isfort, O.; Boddenberg, B.; Fujara, F.; Grosse, R. *Chem. Phys. Lett*. **1998**, *288*, 71.

(8) Schwerk, U.; Michel, D. *Colloids Surf., A* **1996**, *115*, 267.

(9) Böhlmann, W.; Michel, D.; Roland, J. *Magn. Reson. Chem*. **1999**, *37*, S126.

(10) Abraham, A. *The Principles of Nuclear Magnetism*; Oxford University Press: London, 1961.

(11) Lipari, G.; Szabo, A. *J. Am. Chem. Soc*. **1982**, *104*, 4546.

(12) Wittebort, R. J.; Szabo A. *J. Chem. Phys*. **1978**, *69*, 1722.

(13) Mehring M. *Principles of High-Resolution NMR in Solids*; Springer-Verlag: Berlin, Heidelberg, New York, 1983.

(14) Fagerness, P. E.; Grant, D. M.; Kuhlmann, K. F.; Mayne, C. L.; Parry, R. B. *J. Chem. Phys*. **1975**, *63*, 2524.

(15) Schmidt-Rohr, K.; Clauss, J.; Spiess, H. *Macromolecules* **1992**, *25*, 3273.

(16) Lee, M.; Goldburg, W. I. *Phys. Rev. A* **1965**, *140*, 1261.

(17) Roland, J.; Michel, D. *Magn. Reson. Chem*. **2000**, *38*, 587.

(18) Fenzke, D.; Gerstein, B. C.; Pfeifer, H. *J. Magn. Reson*. **1992**, 469.

(19) Schmidt-Rohr, K.; Spiess, H. W. *Multidimensional solid-state NMR and polymers*; Academic Press: London, 1994.

(20) Pauls, K. P.; MacKay, A. L.; Söderman, O.; Bloom, M.; Tanjea, A. K.; Hodges, R. S. *Eur. Biophys. J*. **1985**, *12*, 1.

(21) Dong, R. Y. *Nuclear Magnetic Resonance of Liquid Crystals*; Springer: New York, 1997.

(22) Neuhaus, D.; Williamson, M. P. *The Nuclear Overhauser effect in structural and conformational analysis*; VCH: New York, 1989.

(23) Yaws, C. L. *Handbook of viscosity*; Gulf Publishing Company: Houston, TX, 1995.

(24) Magusin, P. C. M. M.; van Santen, R. A. *Chem. Phys. Lett*. **2003**, *373*, 630.

(25) Maginn, E. J.; Bell, A. T.; Theodorou, D. N. *J. Phys. Chem*. **1996**, *100*, 7155.

(26) Chudnovsky, M.; Garanin D. A. *Phys. Rev. Lett*. **1997**, *79*, 4469.

(27) Fenrych, J.; Reynhardt, E. C.; Basson, I. *Chem. Phys. Lett*. **1997**, *275*, 215.

(28) Demontis, P.; Suffritti, G. B. *Chem. Rev*. **1997**, *97*, 2845.

(29) Suffritti, G. B.; Demontis, P.; Ciccotti, G. *J. Chem. Phys*. **2003**, *118*, 3439.

(30) Kopelevich, D. I.; Chang, H. C. *J. Chem. Phys*. **2001**, *114*, 3776.

(31) Fritzsche, S.; Wolfsberg, M.; Haberlandt, R.; Demontis, P.; Suffritti, G. B.; Tilocca, A. *Chem. Phys. Lett*. **1998**, *296*, 253.

(32) Jousse, F.; Auerbach, S. M.; Jobic, H.; Vercauteren, D. P. *J. Phys. IV France* **2000**, 10 Pr7−147.

(33) Fyfe, C. A.; Kennedy, G. J.; De Schutter, C. T.; Kokotailo, G. T. *J. Chem. Soc., Chem. Commun*. **1984**, 541.

(34) van Koningsveld, H.; Tuinstra, F.; van Bekkum, H.; Jansen, J. C. *Acta Crystallogr*. **1989**, *B45*, 423.

(35) Jobic, H.; Smirnov, K. S.; Bougeard, D. *Chem. Phys. Lett*. **2001**, *344*, 147.

(36) Edmonds, A. R. *Angular Momentum in Quantum Mechanics*; Princeton University Press: Princeton, NJ, 1960.